Magnetic Field Analysis of the Electrode Arc Furnace in Steel Making Foundries

C. W. Kim* and J. I. Im

Material Processing Center, Research Institute of Industrial Science & Technology (RIST), Pohang 790-600, Korea

Finite element analysis showed that strong magnetic fields were distributed around the arc furnace where the strongest magnetic fields were generated around the three phase cables. The second and third strongest fields near the arc furnace were found to be generated around the electrodes and the mast-arms, respectively. The generated field intensities were greatly influenced by the mast arm structure of the arc furnace as well as the phase differences and operation currents of the supplied power. Magnetic field decay patterns around the arc furnace could be smoothly fitted by this equation of exponential formula, $H=H_0+Ae^{-r}$. These results revealed that magnetic field intensities around the arc furnace could be estimated at any 3-dimensional position using finite element method (FEM).

Key words : FEM, arc furnace, equi-magnetic contour line, magnetic field distribution

1. Introduction

The arc furnace is an important electric power machine in steel making foundries. But this machine generates the strong magnetic fields by using high electric power during operation and has many inherent problems to be solved. Problems encountered in the arc furnace foundry are inducing eddy currents on the surface of the construction of iron materials, sparking on the hand rails installed near the arc furnace, AC interference on monitor screens in the operation room, etc. Strong magnetic fields produced by electric arc furnaces installed at the foundry are believed to cause these problems. Also, public concerns about the possible health risks that may result from the magnetic fields have increased during past years. But, few studies [1-3] have reported magnetic field analyses around high electric power machines, such as the arc furnace. Systematic studies are needed to solve the problems described above.

In this study, we have performed the magnetic field study using the finite element method in order to get the information on the magnetic field distribution of the arc furnace by measurements and analytical model calculations. We have also derived an approximate equation to estimate the field intensity at any 3-dimensional position using finite element analysis.

*Corresponding author: Tel: +82-54-279-6332, e-mail: cwkim@rist.re.kr

2. Magnetic Field Analysis

2.1. 3D FEM Analytical model

A 3-dimensional analytical model was constructed by describing the components of the arc furnace installed at POSCO's steel making foundry, such as 3-phase cables, mast-arms, 3-phase electrodes, floor plates and shielding plates, as shown in Fig. 1. The model contained an air layer to surround the arc furnace. The model dimensions were 20 m (X) × 30 m (Y) × 15 m (Z). The coordinate Z represents the model's height and coordinates X, Y represent the length and width, as presented in Fig.1. In order to maintain sufficient accuracy of the finite element model for calculation, the adaptive meshing technique was used in describing the analytical model. The established finite element model consisted of approximately 15,000 elements and 400,000 nodes with the following calculation conditions: an infinite boundary condition was applied to 6 planes of the model, and interfaces of molten metal contacted with the slag layer in the ladle and the ladle shell were electrically grounded. A current was set to flow through 3-phase cables, followed by the mast-arms and 3-phase electrode.

2.2. Magnetic field distribution

To determine the magnetic field distribution around the arc furnace, the well-known ANSYS 5.7 S/W, 3-D magnetic field analyzer was used to perform harmonic analysis for
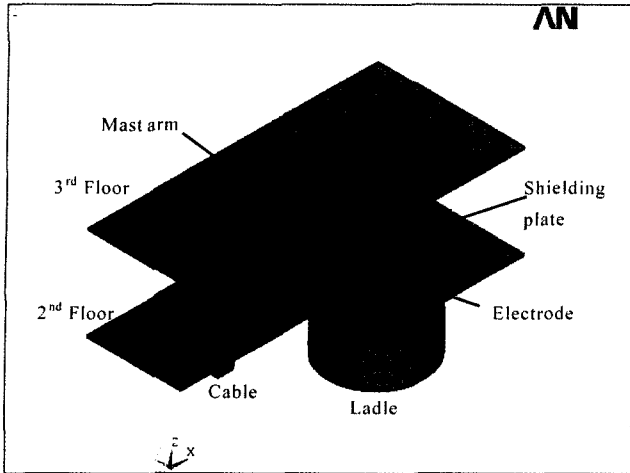
Fig. 1. Analytical model of the arc furnace.

a fixed frequency of 60 Hz. Maxwell's equation for the dynamic state condition for an input AC current of 60 Hz was solved by FEM [4, 5] as an approximate method for solving differential equations at given initial and boundary
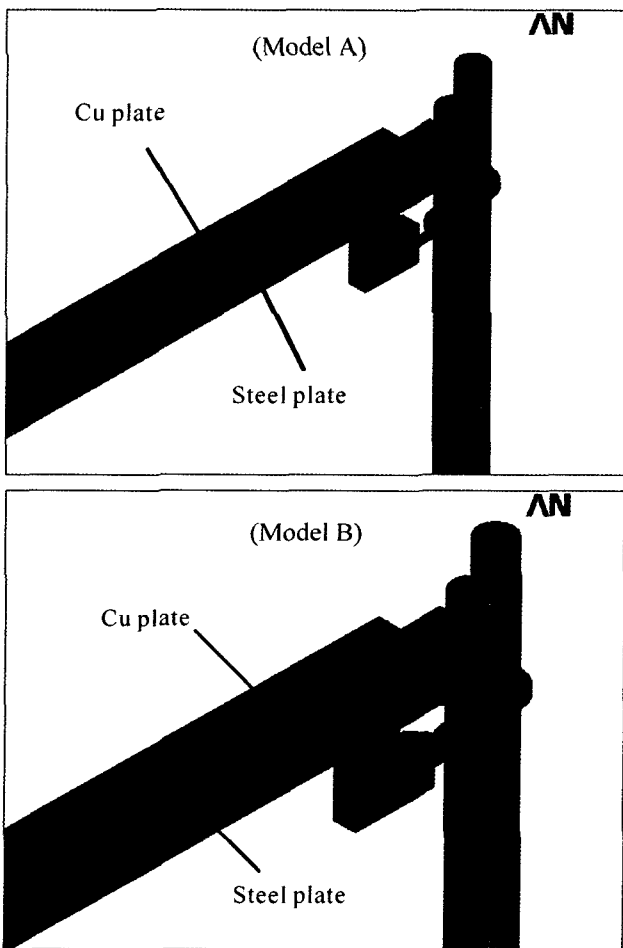

Fig. 2. Mast-arm structure of model A and model B.

Table 1. Input data for 3-D analysis

Components	Resistance (Ωm)	Permeability
Concrete wall	1.0×10^{15}	1
Graphite electrode	4.0×10^{-4}	1
Mast arm	1.0×10^{-7}	200
Rubber cable	1.0×10^{15}	1
Conduction wire	1.7×10^{-8}	1
Floor, shielding plate	1.0×10^{-7}	200
Air	1.0×10^{15}	1

conditions. Magnetic analysis was carried out to investigate the dependency of current and phase difference on field distribution. In addition, magnetic analysis was performed for the two different cases in mast-arm structure as shown in Fig. 2. The Cu-plated conductor was formed at the inside and the outside of the steel plate in mast-arm in case of model A and model B, respectively. The input permeability and resistance of various materials for calculations were presented in Table 1. From the analysis results, 3D-magnetic vector potential; magnetic flux density; magnetic field distribution; and 2D equi-magnetic field contour lines, to aid in interpretation, were obtained.

3. Results and Discussion

3.1. Analysis of magnetic field distribution

Fig. 3 demonstrates the 2-dimensional equi-magnetic field contour lines (X-Y plane) around the arc furnace with a 45 kilo-amperes (kA) load current and a phase difference of 120 degrees. Strong magnetic fields were generated by the magnetic sources (3-phase cables, mast-arms and 3-phase electrodes). Magnetic fields distributed
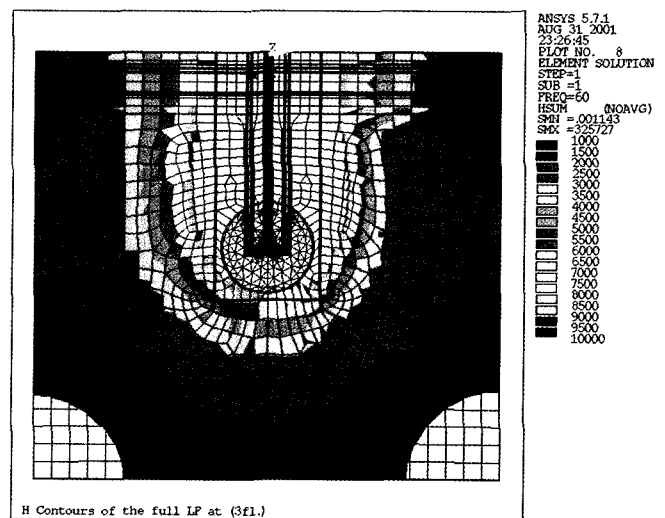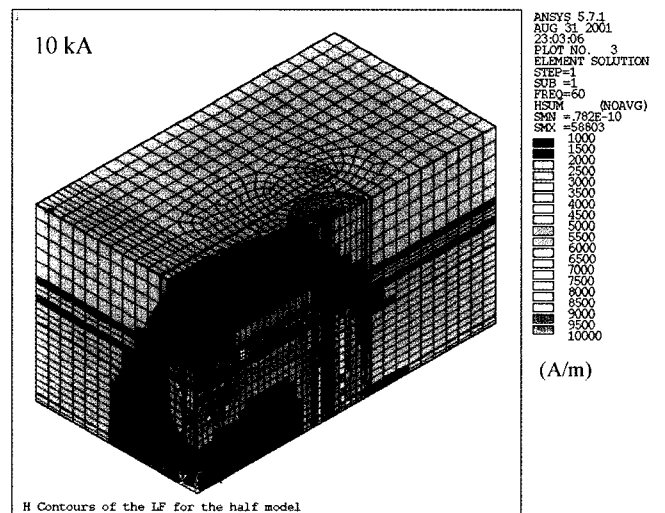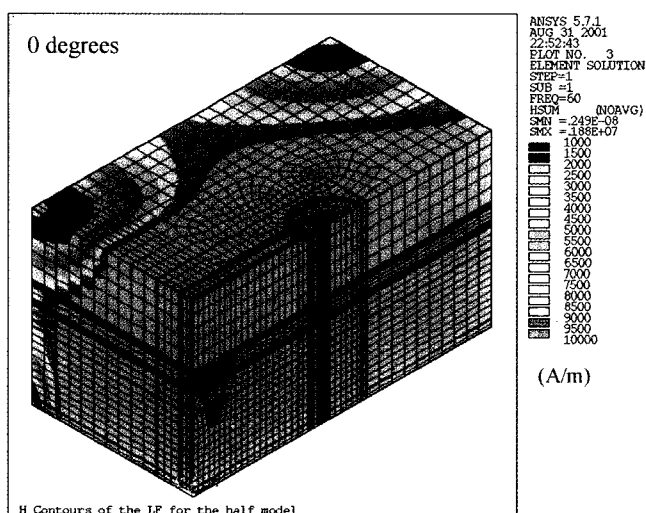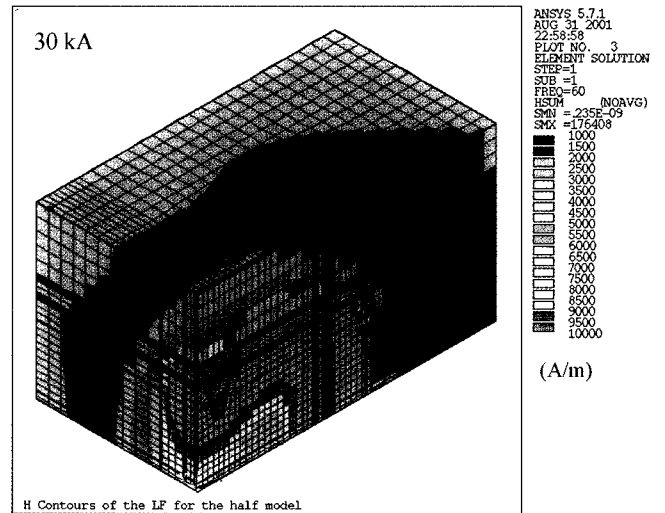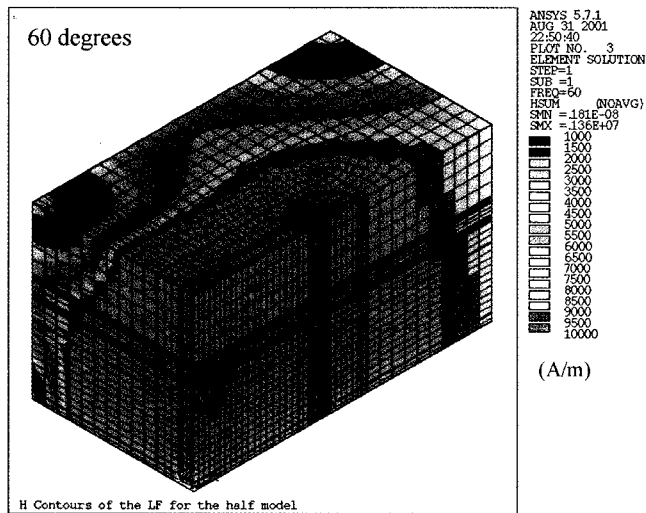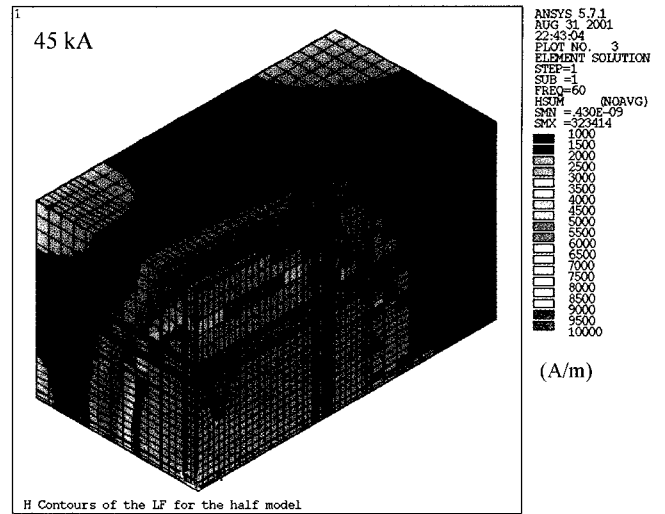

Fig. 3. 2-D equi-magnetic field contour lines (X-Y plane) at the 2nd floor of the arc furnace.
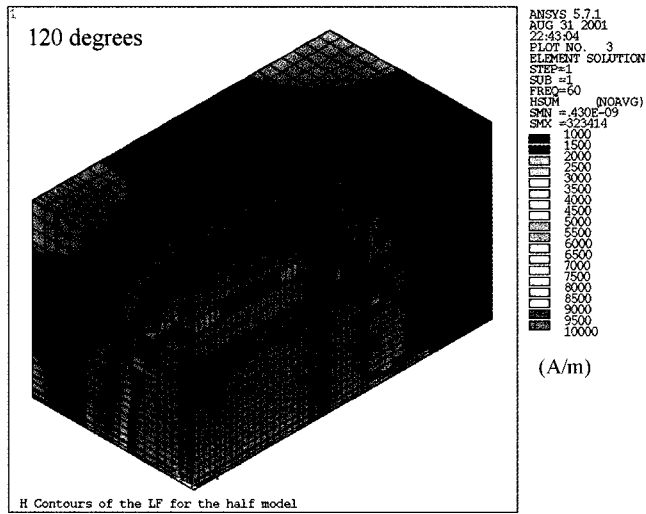
Fig. 4. Dependence of the field intensity on the phase difference between three-phase currents.

Fig. 5. Dependence of the field intensity on the conductor's current.

around the mast-arms were symmetrical.

In order to investigate the magnetic field distribution

effect of the 3-phase differences, the field calculations were carried out at 120, 60 and 0 degrees, with a fixed

current of 45 kA. The results are presented in Fig. 4. The weakest magnetic field was observed when the phase difference was 120 degrees. The strongest magnetic fields were found around the magnetic sources when the phase difference was 0 degrees. The magnetic fields at a distance of 6 meters from the center point of the arc furnace with a phase difference of 0 degrees was about 5 times stronger than the phase difference was 120 degrees. This result indicates that the counterbalancing effect originated from the magnetic vector direction of the fields generated by each 3-phase conductor was significantly lessened, compared to that of the other cases.

In order to investigate the effect of the load currents in calculations on the magnetic field distribution, the field calculations were performed with load currents of 10, 30 and 45 kA, and a phase difference of 120 degrees. From

the calculation results presented in Fig. 5, it is thought (and was predicted) that magnetic fields generated by magnetic sources become stronger as the load current increases. The magnetic field around the center of the arc furnace with a load current of 45 kA was about 6 times stronger than with a current of 10 kA. Figs. 3~5 were calculated data for Model B which was employed in the commercialized arc furnace installed at steel making foundries.

Fig. 6 shows the magnetic vector plots of the field calculations (at 45 kA and 120 degrees) for the cross-section of mast-arm in model A and model B, with structural differences in the mast-arm of the arc furnace shown in Fig. 2. Comparing the magnetic vector plot of model A with that of model B, it is found that the magnetic field generated by model A is stronger than that of model B, and the magnetic field of model A around mast-arms is about 3 times stronger than that of model B. This is considered to be associated with the counter-balancing effect as described above. Further study is in process using the analytical model of mast-arms to examine the details of the results.
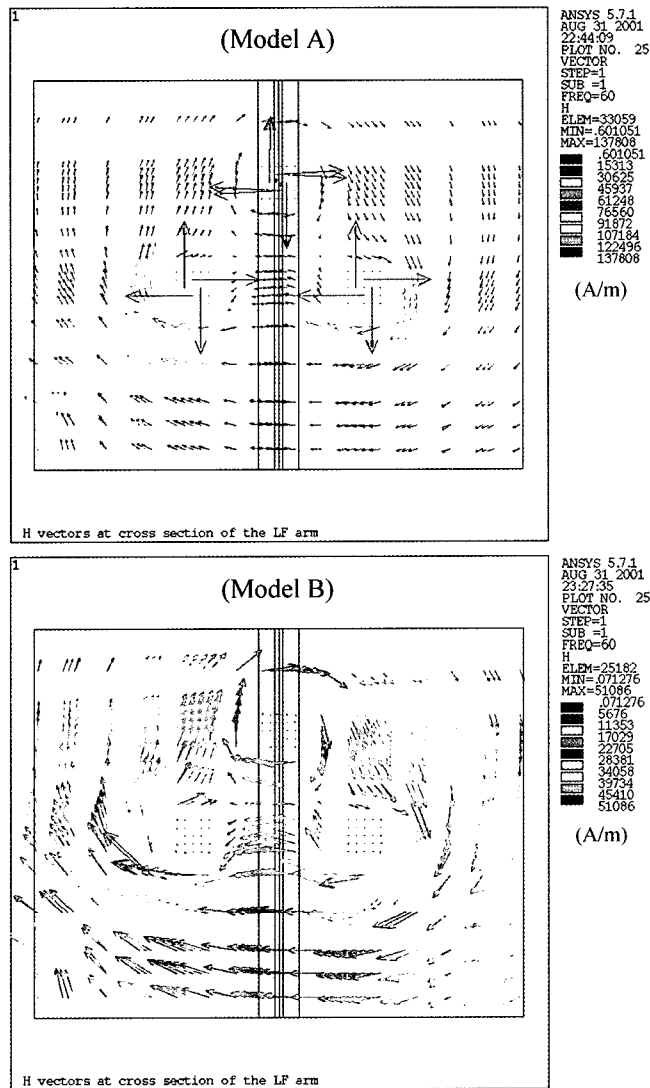
3.2. Field Formulation

In order to derive the approximate equation for the formulation of the field distribution around the arc furnace operated at a load current of 45 kA in the present
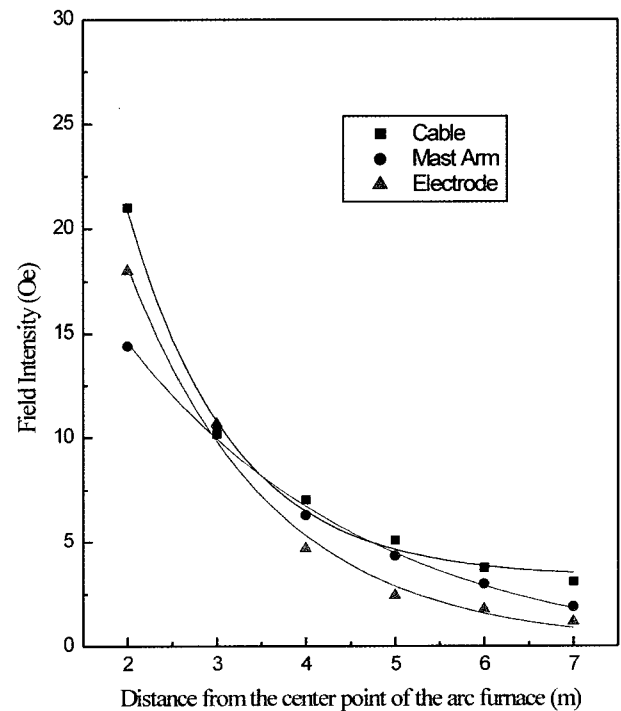

Fig. 6. Comparison between the field distribution of model A and that of model B.

Fig. 7. Dependence of the measured field intensity on the distance from the magnetic source.

Table 2. Decay constants and amplitudes of the measured field profiles

Position Varaiables	Cable		Mast-arms		Electrode	
	fitting	re-fitting	fitting	re-fitting	fitting	re-fitting
B_0 (offset)	3.278	0	-0.706	0	0.0465	0
A (ampl.)	96.53	84.47	31.43	30.1	62.54	62.45
t (decay const.)	1.174	1.515	2.776	2.801	1.619	1.625

study, the fitting method was used in analyzing magnetic field data with measurements as well as with FEM calculations. To formulate the field decay in simple patterns, fitting was carried out by the following exponential formula.

$$H = H_0 + A e^{-\frac{r}{t}} \quad (1^{st}\ \text{order}) \tag{1}$$

where "H" is the magnetic field at a distance of "r" from the center point of the arc furnace and "H_0" is offset value. "A" and "t" are the decay amplitude and the decay constant, respectively.

Magnetic field was measured at POSCO's steel making foundry for 3-phase cables using the three-axial field survey meter in the vertical direction of mast-arms (Y direction) at 1-meter intervals from the center point of 3-phase cables, whose coordinate in FEM model was X=1 m, Y=0 m and, Z=12 m. Also, field measurements were performed in same manner for the mast-arms (X=7 m, Y=0 m and, Z=12 m) and 3-phase electrodes (X=11 m, Y=0 m and, Z=12 m) as were done for the 3-phase cables. The arc furnace was operated at load currents of 45 kA and a phase difference of 120 degrees.

Fig. 7 shows the measured values and the fitting results (solid lines) for the fields generated by 3-phase cables, mast-arms and 3-phase electrodes. The observed magnetic fields were decayed in similar patterns for 3-phase cables, mast-arms, and 3-phase electrodes. The strongest magnetic fields were found around three phase cables. The magnetic fields of electrodes were weaker and the mast-arm magnetic fields were the weakest within about 3 meters from the center point of the arc furnace.

As was predicted in Biot-Savart's law [6], magnetic fields converge to "0" as the distance from the magnetic sources goes to infinity. Therefore, measured data was re-fitted by trial and error to make offset values "0" by controlling the decay constants and the decay amplitudes. The results are presented in Table 2.

Fig. 8 shows the calculated field intensities in Y direction from each center point of 3-phase cables, mast-arms and 3-phase electrodes, whose coordinates are the same as those of the measured points. Field distributions of the
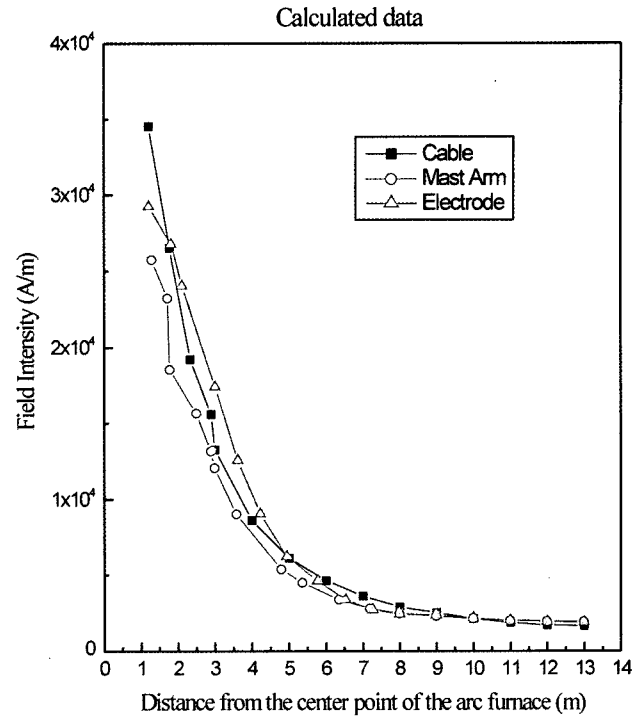
Fig. 8. Dependence of the calculated field intensity on the distance from the magnetic source.
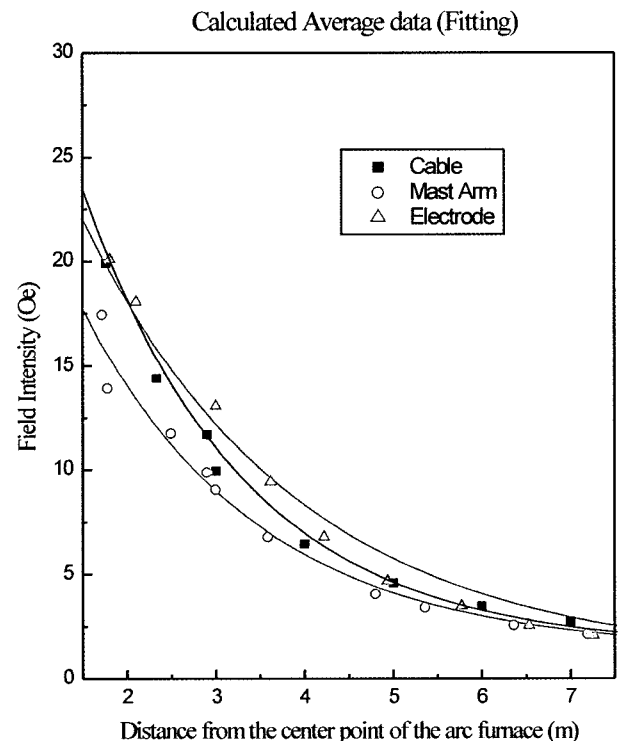
Fig. 9. Fitting profiles of the calculated field intensity around the arc furnace.

calculated data were similar to those of the measured data and the decreasing order of the calculated data in mag-

Table 3. Comparison of the decay constants and amplitudes of the calculated results with those of the measured data

Position Varaiables	cable		Mast-arms		Electrode	
	Meas.	Cal.	Meas..	Cal.	Meas.	Cal.
B_0 (offset)	0	1.427	0	0.753	0	1.306
A (ampl.)	84.47	47.41	30.1	37.78	62.45	35.06
t (decay const.)	1.515	1.829	2.801	2.441	1.625	1.983

netic fields was also found to be similar to that of the measured data near the magnetic sources.

When comparing the results of Fig. 8 with that of Fig. 7, field decay patterns of the calculated values agree very well with those of the measured ones. Therefore, in order to derive an approximate equation for the field decay from the arc furnace, the scales of Fig. 8 were converted into the new scales of Fig. 7 by multiplying them with a conversion factor, 7.5×10^{-4}. Fittings were made on the results after converting the scale. Fig. 9 shows the fitting results. The decay constants and decay amplitudes after fitting are presented in Table 3. Decay constants and decay amplitudes of the measured data were found to be similar to those of the calculated data from Table 3. Error calculations show that the calculated magnetic field around 3-phase cables, mast-arms and 3-phase electrodes agreed with the measured ones, within the error limits of 10%, 14% and 22%, respectively. For the estimation of the calculation accuracy, field measurement was carried out at the arc furnace operated at the same working condition described above. The measured field at 15 m from 3-phase cables was observed to be about 50 mG. This value was closed to the calculated data using the approximate equation (1). From the results, it can be concluded that the magnetic fields at a certain position from the arc furnace can be predicted using the finite element analysis.

4. Conclusions

1) Finite element analysis showed that strong magnetic fields were distributed around the arc furnace where the strongest magnetic fields were generated around the three phase cables. The second and third strongest fields near the arc furnace were found to generate around the electrodes and the mast-arms, respectively. This tendency is similar to the measurement results.

2) The factor that influenced the magnetic field distribution the most in the field calculations was phase difference of input power, followed by the current and the structure of mast-arms in sequential order. The magnetic field generated by model A was stronger than that by model B, and the model A's magnetic field around the mast-arms was 3 times stronger than that of model B. These results indicate that field generated by the arc furnace can be diminished by changing the structural design of mast-arms.

3) When comparing the measured data with the calculated data using equation (1), the calculated magnetic field around 3-phase cables, mast-arms and 3-phase electrodes agreed with the measured ones within the error limits of 10%, 14% and 22%, respectively.

From the results, it can be concluded that magnetic fields at certain positions from the arc furnace can be estimated using the finite element analysis.

References

[1] C. W. Kim and D. C. Lee, Korean J. of Materials Research **9**, 251 (1999).

[2] T. Keikko, J. Isokorpi and L. Korpinen, IEEE Conference Publication **2**, 111 (1999).

[3] Y. Sakai and A. Yamasita, JSME Int. Journal Series A **38**, 52 (1995).

[4] J. L. Volakis, A. Cbatterjee and L. C. Kempel, Finite Elements Method for Electromagnetics, IEEE Press 157 (1998).

[5] E. R. de A. Oliveira, Int. J. of solids Structures **4**, 929 (1968).

[6] J. D. Kraus, Electromagnetics, 3rd ed., McGraw-Hill, New York (1987) pp. 153.